MIEEG-GAN: Generating Artificial Motor Imagery Electroencephalography Signals

Sujit Roy (Roy-s2@ulster.ac.uk), Shirin Dora, Karl McCreadie and Girijesh Prasad

Intelligent Systems Research Centre, School of Computing, Engineering and Intelligent Systems, Ulster University, Londonderry, UK

Abstract—Generative Adversarial Networks (GAN) have led to important advancements in generation of time-series data in areas like speech processing. This ability of GANs can be very useful for Brain-Computer Interfaces (BCIs) where collecting large number of samples can be expensive and time-consuming. To address this issue, this paper presents a new approach for generating artificial electroencephalography (EEG) data for motor imagery. GANs here use a generator and discriminator networks that consist of Bidirectional Long Short Term Memory neurons. Trained models are evaluated using the dataset 2b from the BCI competition IV. The dataset consists of trials with left and right hand motor imagery. Separate GANs are trained to generate artificial EEG samples corresponding to the two types of trials present in the data set. For the purpose of evaluation, the time-frequency characteristics of the real and artificial EEG signals are compared using Short-Term Fourier Transform and Welch's power spectral density. The results indicate that GANs can capture important characteristics of motor imagery EEG data such as power variations in the beta-band. The power variation in the artificial generated and original signal was in the similar frequency bin when looked at Welch's power spectral density.

I. INTRODUCTION

An Electroencephalography(EEG)-based Brain-Computer Interface (BCI) has the potential to allow communication and control for those with severe neuromuscular disorders such as those with amyotrophic lateral sclerosis or more recently for those with a disorder of consciousness. BCI has existed in some form for several decades and although our understanding of machine learning techniques has increased in recent years, due in part to our access to increased computing capacity, progress has still been slow. Performance has improved with advancements in every stage of the signal processing chain from preprocessing to feature extraction and selection through to classification and post-processing [1].

One critical issue is the large number of trials typically required by machine learning models needed to produce a reliable classification. Data collection sessions can be long and tedious affairs but are usually necessary to produce a sufficiently large dataset. However, as this is not always possible due to often complex needs of the patient, researchers are often forced to perform their analyses on datasets which do not allow for the development of adequately robust classifiers.

Deep learning is one machine learning technique used to learn from unstructured data and has demonstrated significant performance in application areas as diverse as drug discovery, language processing and fraud detection. However, the usefulness of this method can be hampered due to the lack of sufficiently large datasets [2].

In BCI, as it is often difficult and expensive to collect the required number of samples; what is needed, is a method for the automatic generation of artificial EEG trials to augment existing datasets. Lotte et al. [3] recently proposed several methods for the artificial generation of EEG trials through the combination and distortion of the real samples, whilst Dinares-Ferran et al. [4] applied the increasingly popular Empirical Mode Decomposition (EMD) to produce artificial EEG frames. Although both these studies considered features in the time and/or frequency domain, Fang et al. [5] used a differential entropy feature which is more applicable to deep computational models.

A recently developed machine learning technique called Generative Adversarial Networks (GANs) [6] which employs deep learning architectures, is gaining increasing attention from the research community due to its relatively simple implementation and promising results in a range of domains. GANs work by training two competing neural network sub-models to produce new data with statistically significantly different characteristics to the training dataset. Until now GANs have mostly been applied to image generation, though there are some examples of their effectiveness for time-series problems [7], [8]. Although there is an increasing number of papers being published using adversarial models [9], their potential for generating artificial EEG signals has not been thoroughly explored.

This study aims to reduce EEG data scarcity and hence address the over-fitting issue commonly faced by BCI researchers by producing a GAN architecture based on Bi-LSTM. LSTM based networks have been used for classification of time-series data like speech signals [10], [11]. The generation of artificial EEG trials will help to reduce both the time and cost of data collection without inconveniencing the patient.

The remainder of the paper is organized as follows: section-II gives a background of the problem statement, dataset description and explanation of the GAN. In Section III, results of evaluation are presented. A discussion of results in presented in Section IV.

II. METHODOLOGY

A. Dataset Description

BCI competition IV-2b is a well-known dataset and is used as a benchmark for testing new algorithms in the area of
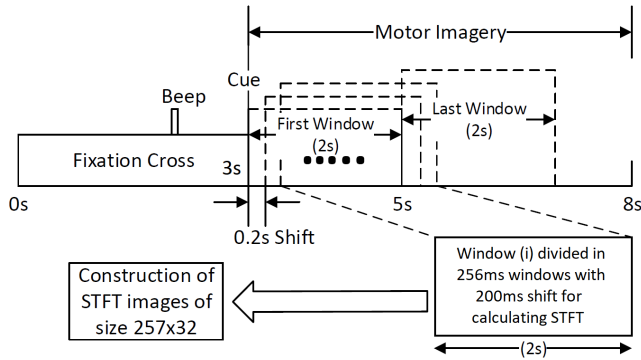
Fig. 1: Construction of STFT images by sliding window of the size 2 s with a shift/hop of 200 ms is divided into 256 ms sub-windows (with 56 ms shift/hop) for calculating STFT the motor-imagery period within the trial.

Fig. 2: Example of a GAN Architecture.

motor imagery-based BCI [12]. It comprises bipolar EEG data recorded from 9 healthy participants in 5 sessions at a sampling rate of 250 Hz. Each session consists of equal number of trials for left hand and right hand motor imagery. The dataset consists of recordings from three channels located over the primary motor cortex (C3, Cz, and C4). The EEG signals from these channels are band-passed between 0.1 and 100 Hz with a notch filter at 50 Hz at the time of recording using the signal acquisition hardware.

Figure 1 shows the timing diagram for a single trial. Each trial starts with an acoustic beep and a fixation cross shown on a blank screen for 3 s followed by a cue. The duration of the cue is 1.25 s in two sessions and is 4.5 s in other sessions. The cue can either be a leftwards or rightwards pointing arrow which instructs the participant to perform left or right-hand motor imagery, respectively for a period of 4 sec. There is an inter-trial interval of 1-2 s. The dataset was originally created for building classifiers that differentiate between the activity performed by the participant based on EEG recordings. For this purpose, the data from first three sessions is designated for training a classifier and the data from other sessions is meant for evaluating the performance of the classifier. In line with this, no feedback is provided in the first three sessions whereas a happy or sad smiley is shown during the motor imagery period in the last two sessions. In this study, we have only used data recorded on the channel C3 in first 3 sessions resulting in a total of 420 trials.

The data from the motor imagery period (between 3 to 7 s) in each trial was divided into multiple samples each of which has a duration of 2 s. The first sample consisted of data recorded within a window of 3 to 5 s on a trial. This window was shifted in steps of 200 ms to obtain the other samples from this trial. Therefore, each trial resulted in generation of 11 samples each of which had a length of 500 (sampling frequency of the EEG signal is 250 Hz). These samples are used for training a GAN.
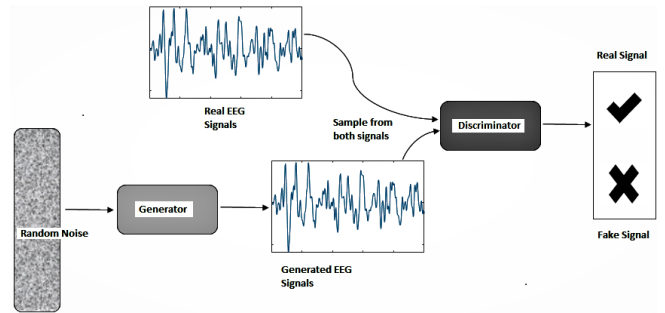
B. Short Term Fourier Transform (STFT)

The STFT is a type of time-frequency distribution [13] consisting of frequency and phase content of local sections of a signal as it changes over time [14], [15], [16]. The STFT can be described mathematically as,

$$X_m(w) = \sum_{n=-\infty}^{\infty} x(n)w(n-mR)e^{-jwn} \quad (1)$$

where $x(n)$ is the input signal at time n, $w(n)$ is the length M of hamming window, $X_m(w)$ is the discrete Fourier transform of windowed data and R is the hop size.

For comparison, STFT is used for obtaining the time-frequency spectra of the motor imagery related changes in the EEG signal. We have chosen a window size of 64 samples, with an overlap of 50 samples between the consecutive windows. The number of fast-Fourier-transform (FFT) points was 512. Thus the size of the spectrogram was 257×32, where 257 was the number of frequency components and 32 was the number of time points. From this spectogram, we choose beta-spectrogram for 13-32 Hz, which was of the size 41×32. Thus the spectrograms of size 40×32 are calculated for each of the three EEG channels C3. This construction process of the STFT images and signal is shown in Fig. 1.

C. Generative Adversarial Network (GAN)

A GAN [6] consists of two different neural networks termed as a generator and discriminator. The aim of the generator, denoted by G, is to capture the distribution of a given dataset, $\mathbf{X} = \{x_1, \cdots, x_i, \cdots\}$, in order to generate novel samples from this distribution. The goal of the discriminator, denoted by D is to differentiate between "real" input samples and "fake" samples produced by the generator. The input for G is $z \in R^M$, an M-dimensional sample from standard normal distribution and its output is a sample $\tilde{x}$ based on the distribution represented by G. The discriminator receives either a sample from $\mathbf{X}$ or a sample produced by the generator and predicts whether the sample is real or fake.

Two networks in GAN are trained in parallel using a loss function of the type given below:

$$\mathbb{L}(G,D) = \mathbb{E}_x[\log D(x)] + \mathbb{E}_z[\log(1 - D(G(z)))] \quad (2)$$
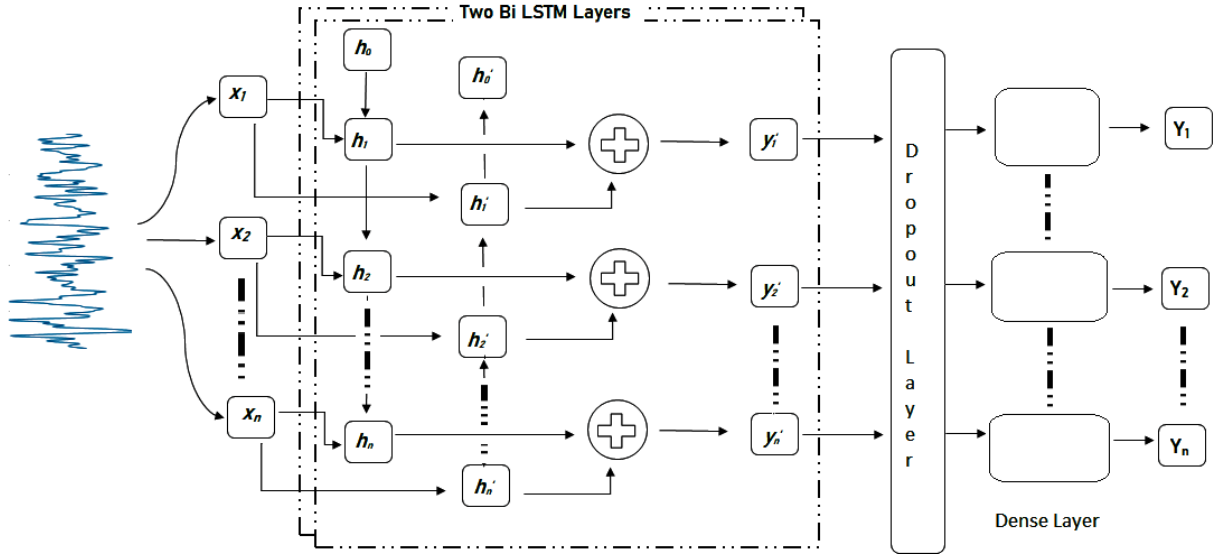
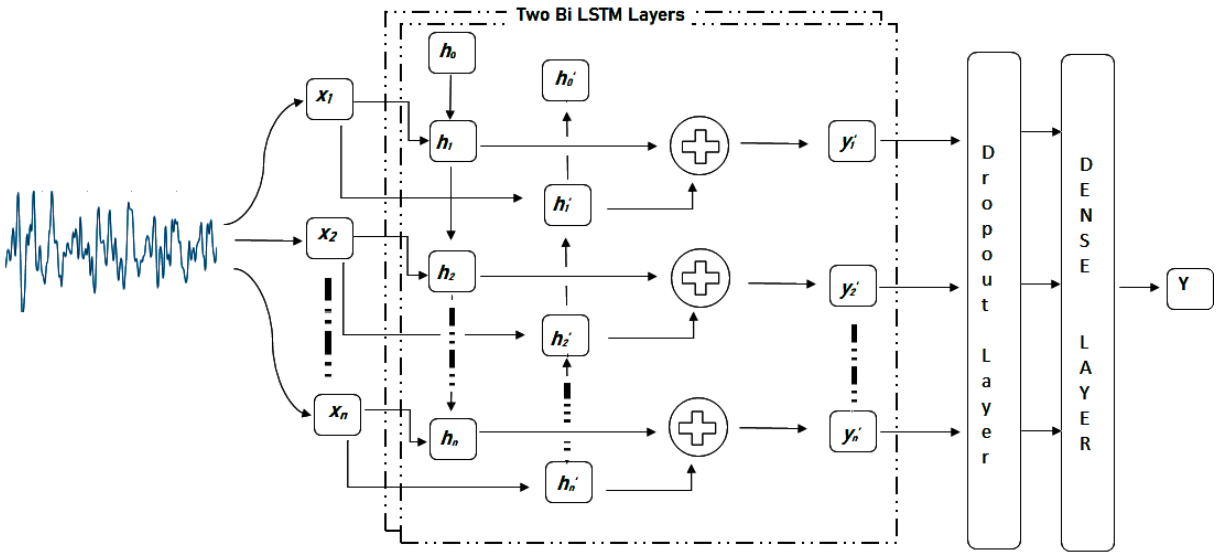Fig. 3: Design of the Generator Architecture.

Fig. 4: Design of the Discriminator Architecture.

The discriminator is trained to minimize this loss function whereas the generator is trained to maximize this loss function thereby acting as an adversary to the discriminator. Generator tries for density estimation, from the noise distribution to the original/real distribution.

The loss function of the Generator is

$$\nabla_{\theta_g} \frac{1}{m} \sum_{n=1}^{m} log(1 - D(G(z^{(i)})))$$ (3)

The loss function of the Discriminator is

$$\nabla_{\theta_d} \frac{1}{m} \sum_{n=1}^{m} [logD(x^{(i)} + log(1 - D(G(z^{(i)}))))]$$ (4)

The first term in Eq 4, is a representation of real data to the generator, where the D will try to maximise the log probability for data to be real, i.e. close to 1. The second term

uses the samples produced by G from noise, where D will try to maximise the probability of prediction close to zero as the data is fake. G tries to minimize the log probability of D for corrections i.e. close to 1 on fake samples.

D. Architecture

We propose a new GAN-based architecture for generating artificial EEG signals. Figure 2 illustrates the architecture of GAN. Similar to the traditional GAN, our model has two neural networks known as a generator and a discriminator. The generator receives an input of 50 noise points which follows Gaussian normal distribution. The output of the generator is of 500 sample points which represents 2 s EEG signal sampled at 250 Hz. The discriminator receives the real and generated EEG signal samples of length of 500 and the output is the representation of probability of real or fake

signal , i.e. $D(x) \in \{0, 1\}$. For the training, the objective is to train D to maximise the probability of identifying the correct label of both the real data points and generated data points.

1) Generator: We provide to the generator with 50 noise data points which follow a Gaussian distribution as a fixed length sequence. Firstly, an input layer is added which takes the GAN input as the number of time steps and noise length. As the length of the signal is 2 s and the sampling frequency is 250 Hz, the time steps will be 500. The generator will have a 2D matrix as an input $[T, D]$, where T is the number of time steps and D is the dimension of noise. Then two Bi-LSTM layers were added with 30 cells each and keeping their return sequence as true. Thus, the output of the first Bi-LSTM layer will be in the shape of [500, 60]. The second Bi-LSTM layer will also have the same output. After this a dropout layer was added followed by a dense layer with 1 neuron for every T. The architecture of the generator is shown in Fig. 3. The Table I shows the parameters of the generators designed for the study.

TABLE I: Parameters for Generator

Layers	Output Shape	Param	Activation
Input	[B, 500, 50]		
Bi-LSTM 1	[B, 500, 60]	19440	tanh
Bi-LSTM 2	[B, 500, 60]	21840	tanh
Dropout	[B, 500, 60]	0	
Dense	[B, 500, 1]	61	tanh
Total params : 41,341			
Trainable params : 41,341			
Non-trainable params : 0			

B= Batch Size

In our model, the current hidden state depends upon the forward LSTM and backward LSTM. To calculate the hidden state from forward LSTM we use Eq (5) and for backward Eq (6). To have the Bi-LSTM with L layers, where the input at every intermediate neuron at level i will be the output of the Bi-LSTM at layer $i - 1$ at the common time-step, t. The output $\hat{y}$ at every time-step is the result of propagating input through all layers Eq(7).

$$\vec{h}_t^{(i)} = tanh(W_{i\vec{h}}^{(i)} x_t + W_{\vec{h}\vec{h}}^{(i)} \vec{h}_{t-1}^{(i)} + b_{\vec{h}}^{(i)}) \qquad (5)$$

$$\overleftarrow{h}_t^{(i)} = tanh(W_{i\overleftarrow{h}}^{(i)} x_t + W_{\overleftarrow{h}\overleftarrow{h}}^{(i)} \overleftarrow{h}_{t+1}^{(i)} + b_{\overleftarrow{h}}^{(i)}) \qquad (6)$$

$$\hat{y}_t = tanh(u[\vec{h}_t^{(L)}; \overleftarrow{h}_t^{(L)}] + c) \qquad (7)$$

The activation function for all the Bi-LSTM layers was *tanh*. The loss function for generator was categorical cross entropy.

2) Discriminator: The design of the the discriminator was similar to the generator except the last layer was used with one output neuron as a dense layer for classification of real vs. fake image. The first layer is the input layer which will have an input of signal of sample length of 500, followed by

two Bi-LSTM layers with 30 cells each. After this a dropout layer was added and a dense layer was also added with one output neuron. The activation function for the two Bi-LSTM layers were *tanh* and for dense layer it was *sigmoid*. The loss function for discriminator was also categorical cross entropy. The model was trained for 120 epochs. The design of the discriminator is shown in Fig 4. The table II shows the parameters of the discriminator.

TABLE II: Parameters for Discriminator

Layers	Output Shape	Param	Activation
Input	[B, 500]		
Bi-LSTM 1	[B, 500, 60]	76,800	tanh
Bi-LSTM 2	[B, 500, 60]	21,840	tanh
Dropout	[B, 500, 60]	0	
Flatten	[B, 30,000]	0	
Dense	[B, 1]	30,001	sigmoid
Total params : 59,521			
Trainable params : 59,521			
Non-trainable params : 0			

B= Batch Size

III. RESULTS

In this section, we are going to evaluate the real MI-EEG signals and signals generated by the GAN described in Section II. For comparison we will be looking at power distribution, first/second order characteristics, and STFT spectrograms.

Python 3.x with MNE is used to read the EEG signals and Tensorflow 2.0 framework is used for developing GANs. MATLAB 2019a is employed for analysis and EEG segmentation. All the experiments were conducted in Windows 10 environment on an i7 8th gen processor with an Nvidia RTX2080 Ti GPU.

Figure 5 displays the plot of the raw EEG signal from a single trial of MI-EEG. The Fig. 5(a) represents signal generated artificially from noise by training the GAN for the left hand MI-EEG samples. Fig. 5(c) represents the signal generated from noise by training GAN on the right hand MI-EEG signal. Similarly, Fig. 5(b) and 5(d) represents real EEG signal of left and right hand motor imagery respectively.

A. Dynamic Characteristics of the EEG Signal

We studied the first order characteristics of the generated and original EEG signal. For this purpose we computed the difference between the amplitude of the signal at time t and $(t - 1)$, given by

$$\Delta x(t) = x(t) - x(t - 1) \qquad (8)$$

Fig. 6 shows the plot of $\Delta x(t)$ vs $\Delta x(t + 1)$ for real and artificial EEG. It was observed that both real and the artificial EEG signals exhibited similar relationship between $\Delta x(t)$ and $\Delta x(t + 1)$ (c.f. Fig. 6). This clearly shows that the GAN captures the temporal relationships present in the real
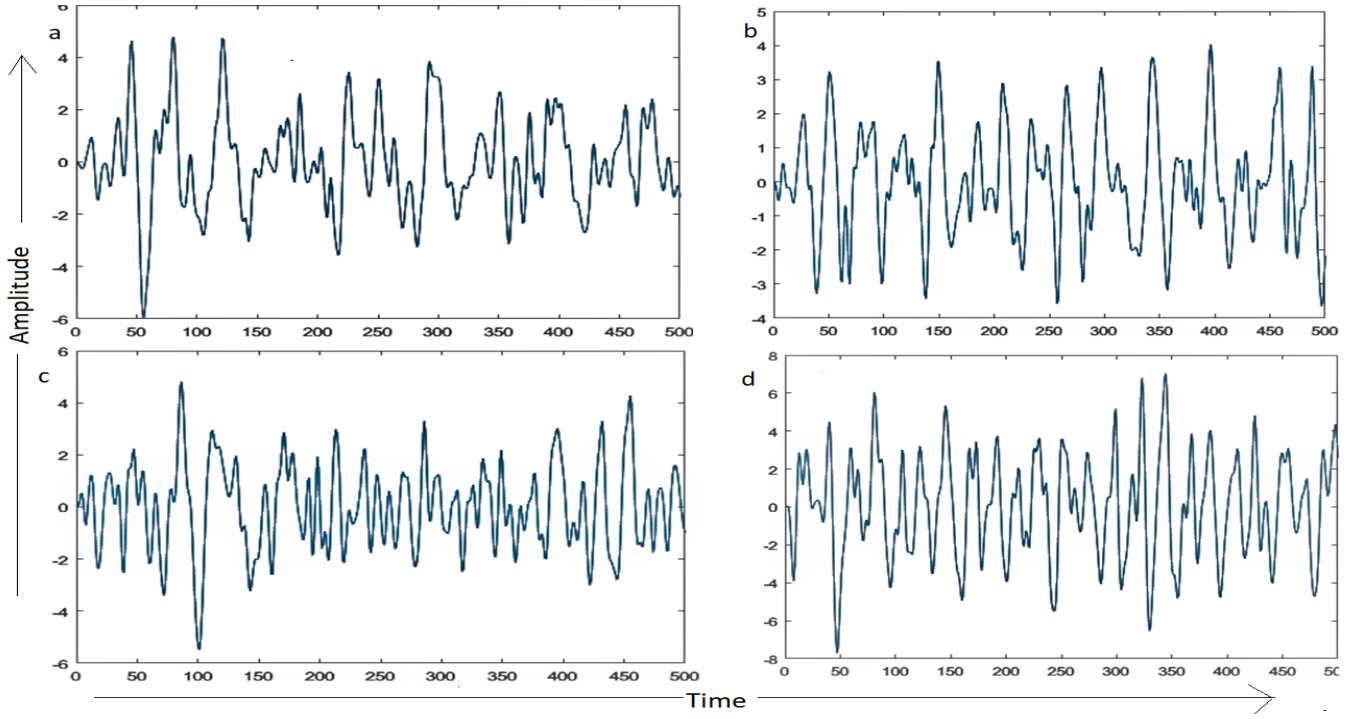
Fig. 5: a) Raw signal of a trial of artificially generated left hand MI-EEG, b) Raw signal of a trial of real left hand MI-EEG, c) Raw signal of a trial of artificially generated right hand MI-EEG, d) Raw signal of a trial of real right hand MI-EEG.
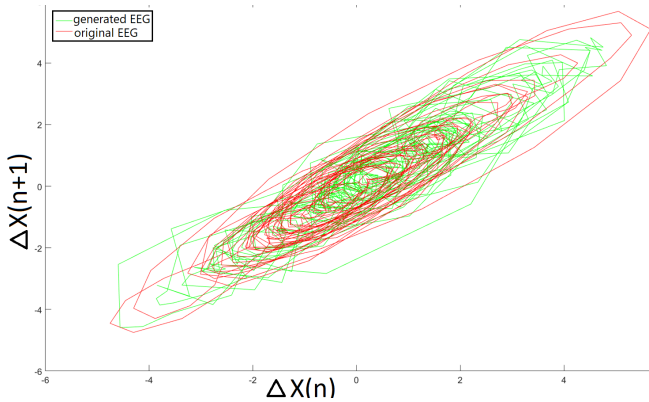

Fig. 6: Example of plot generated for a sample of real and artificially generated left hand MI-EEG signal in beta band(13-40 Hz) using Eq (9).

EEG signal. To describe mathematically, EEG samples can be represented as:

$$\Delta x(n+1) = f(\Delta x(n)) \tag{9}$$

where $x(n)$ is considered as EEG signal representation for the n sample point. This identification was very important for generating artificial EEG as this shows if the generator is able to understand the correlation of next sample point with respect to previous. Fig. 6 shows the plot generated by the Eq (9) for real and artificial EEG. It is to be noted, when we designed the generator with convolution layers we were not able to generate this plot, rather it was random. The fig. 6

clearly shows that the generated EEG signal's sample points are correlated and following the pattern of an ellipse by Eq (9).
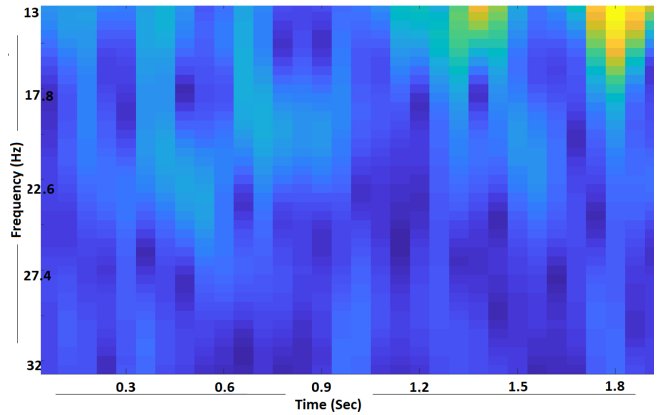

Fig. 7: Example of STFT generated image for real left hand MI-EEG signal in beta band (13-32) Hz).

B. Time-frequency Spectrogram

In this section, we visualize the time-frequency spectrograms of the real EEG data and samples generated by the GAN.

Fig. 7 displays the beta-band spectrogram of a single trial for left hand motor imagery from the real EEG recordings. Fig. 8 shows the beta-band spectrogram of a single sample generated by the GAN for left hand motor imagery. It can

be observed that both real and the generated EEG signals have similar spectrograms in the beta-band. STFT generated from real sample and artificial sample shows very similar activation pattern for left hand imagery. Fig 8 shows some noisy fluctuation in the band of 13-17 Hz. However as, this experiment did not aim for exact image translation and STFT shows some leakage effect, thus some interference of other real samples can be expected as the model will try to learn the variable distribution of different trials which is resulted in noise.
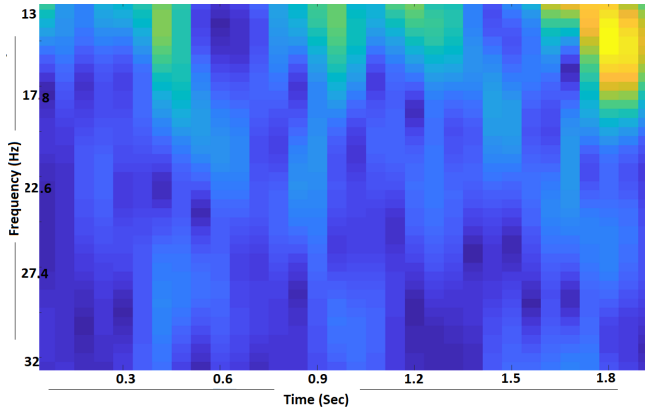
Fig. 8: An example of STFT in beta-band (13-32 Hz) for an artificial EEG signal generated during left-hand MI task.

A similar study is also conducted for right hand motor imagery samples generated by the GAN. Figure 9 shows the beta-band spectrogram during right hand motor imagery of a single real and generated EEG sample, respectively. The activation pattern is similar to that of right hand movement, however, it is also important to notice that there is difference in the STFT generated for left hand and right hand.
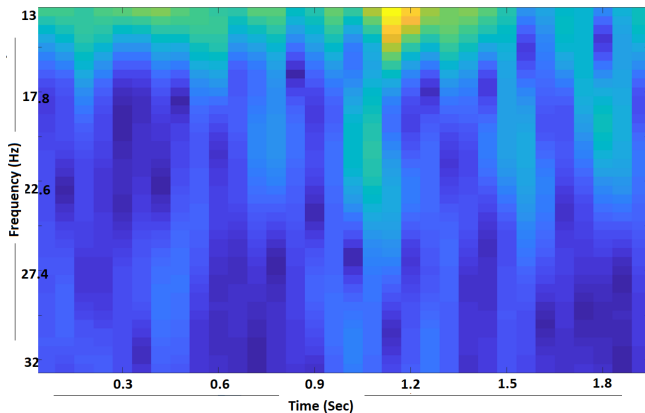

Fig. 9: Example of STFT generated image for real right hand MI-EEG signal in beta band (13-32 Hz).

By looking at the STFT for right hand and left hand separately, some noise was noticed in the the sample length of 2 s. To look at it more carefully, the averages of all generated samples were calculated and then STFT was generated from them. Figure 11 and 12 show the average beta-band
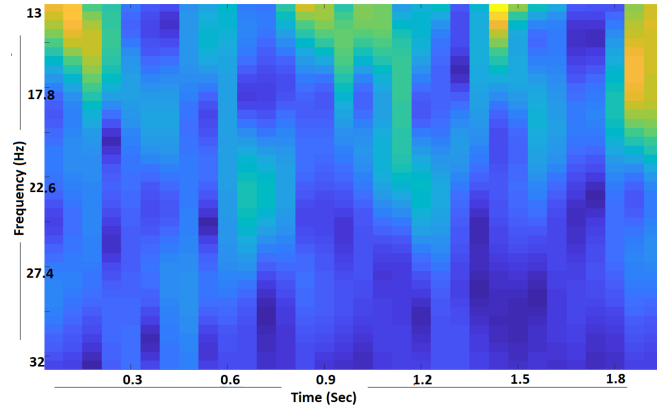

Fig. 10: Example of STFT generated image for artificially generated right hand MI-EEG signal in beta band (13-32 Hz).

spectrogram for 2288 left hand MI samples from real and generated EEG signal, respectively. It may be noted that artificially generated samples of EEG are noisy compared to the real EEG as was suspected. Additionally, the activation in higher β band (22.6-32 Hz) was also amplified a bit compared to real EEG. However, the pattern of β activations present in real EEG can also be observed in the artificially generated EEG.

Fig 13 shows the Welch's power spectral density of real and artificially generated EEG. From the figure the power drop in both can be seen in the similar frequency bin (0-0.6). The distributions of real and artificial EEG are closely followed.
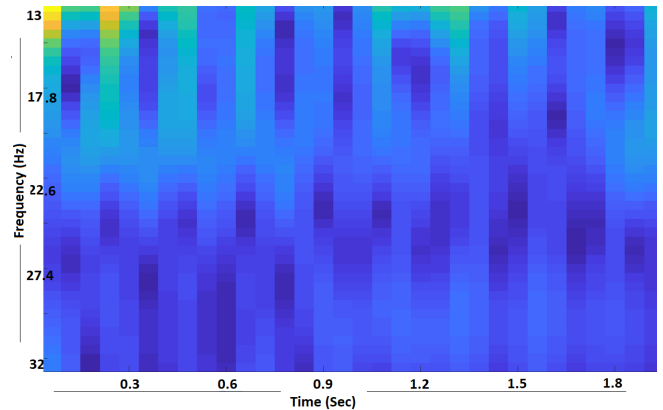

Fig. 11: Example of STFT generated image for real left hand MI-EEG signal. The image is formed by taking the mean of all the trials in the beta band (13-32 Hz) and then calculated STFT over mean signal.

IV. DISCUSSION & CONCLUSION

In this paper, we described a general method for artificially generating motor imagery related EEG signals. The results have focused on EEG signals recorded from a single channel. However, the approach can be easily extended to generate
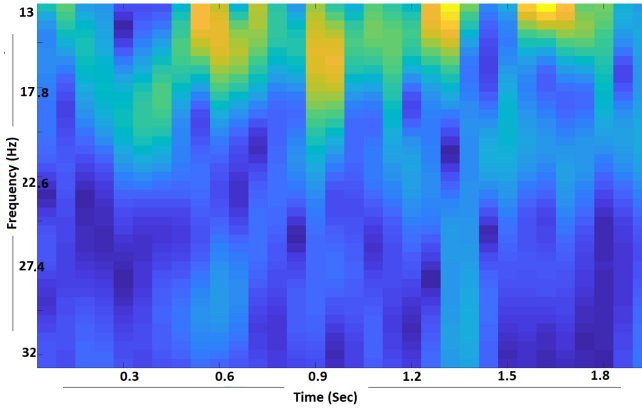
Fig. 12: Example of STFT generated image for artificially generated left hand MI-EEG signal. The image is formed by taking the mean of all the trials in the beta band (13-32 Hz) and then calculated STFT over mean signal.
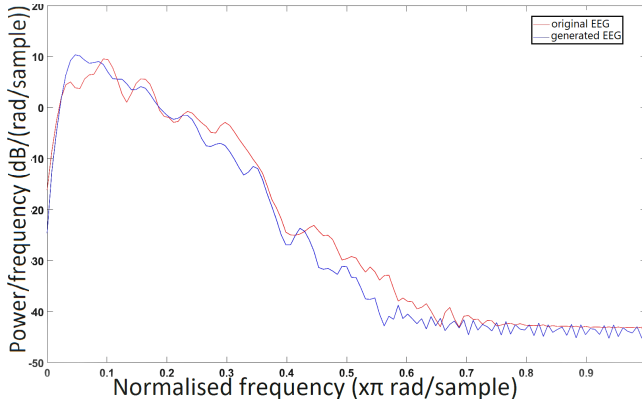

Fig. 13: Welch's power spectral density for real signal and artificial signal of left hand MI-EEG .

EEG signals for multiple channels by following the principles described in this paper.

The spectrograms and the power spectral density analyses clearly show that the artificially generated EEG signal exhibits properties similar to the original EEG signal. Visual inspection of power variations in the lower β band, i.e 13-20 Hz of the artificial and original EEG signal indicated presence of similar patterns. Furthermore, artificial EEG signals for the two classes right hand and left hand show distinct signatures which should be useful from a classification perspective. PSD plot confirms the pattern of power variation in the specified frequency bins for real and artificial signals. These results indicate that GANs can be used to generate artificial EEG signals that have properties similar to properties of the original EEG signals. It is also possible to create an input image by taking STFT of input signal as discussed by [17], which can be used for further artificial generation of STFT spectrograms. However, it would be very difficult to obtain the raw signal from STFT as it will not have its complex parameters to revert to the real signal. Without generation of the raw signal it would not be possible

to explore the other properties of artificial signal for further evaluation.

The signals generated by Bi-LSTM based architecture also express beta oscillations and second order characteristics present in the original EEG signal. However, it was observed that artificially generated EEG signals had lower amplitude compared to the original EEG signal. This may be attributed to the property of the original EEG signal that high amplitude signals appear less frequently in comparison to the low amplitude signals. As a result of this imbalance in the data, GANs are unable to accurately capture the amplitude variations in the original EEG signal as shown in Fig. 14.
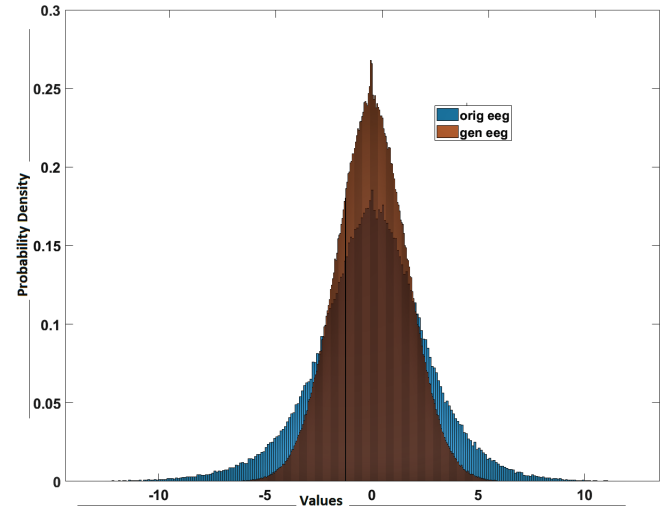

Fig. 14: Plot of probability density function for original and generated left hand MI-EEG data in β frequency band

A convolution-based architecture was also evaluated for generating artificial EEG signals i.e. discriminators and generators designed using 1D/2D convolution. It was observed that the signal generated using the convolution networks was very noisy and didn't follow first order characteristics of the EEG signal. This could be due to the fact that EEG signals are inherently temporally correlated and a convolution based architecture is unable to capture these correlations. While performing 1D/2D convolution simply spatial features of the raw signal are being extracted . On the other hand, an LSTM-based model is inherently designed to capture temporal relationships present in data.

In conclusion, the described model can be used for the generation of artificial EEG signals for motor imagery. However better results can be achieved by having more trials for full motor imagery activity as the model will be able to learn the event related desynchronisation and event related synchronisation (ERD/ERS) patterns as well, which will make the signals more helpful in classification.

V. FUTURE WORK

In this paper, we presented a new GAN-based approach for generating artificial EEG signal. However, the model does not capture very well the amplitude variations in the original

EEG signal. Furthermore, most of the analyses presented in this paper are based upon visual inspection. Future work will focus on addressing these issues in the proposed approach.

REFERENCES

[1] F. Lotte, L. Bougrain, A. Cichocki, M. Clerc, M. Congedo, A. Rakotomamonjy, and F. Yger, "A review of classification algorithms for eeg-based brain–computer interfaces: a 10 year update," *Journal of neural engineering*, vol. 15, no. 3, p. 031005, 2018.

[2] S. Roy, D. Rathee, K. McCreadie, and G. Prasad, "Channel selection improves meg-based brain-computer interface," in *2019 9th International IEEE/EMBS Conference on Neural Engineering (NER)*. IEEE, 2019, pp. 295–298.

[3] F. Lotte, "Signal processing approaches to minimize or suppress calibration time in oscillatory activity-based brain–computer interfaces," *Proceedings of the IEEE*, vol. 103, no. 6, pp. 871–890, 2015.

[4] J. Dinarès-Ferran, R. Ortner, C. Guger, and J. Solé-Casals, "A new method to generate artificial frames using the empirical mode decomposition for an eeg-based motor imagery bci," *Frontiers in neuroscience*, vol. 12, p. 308, 2018.

[5] F. Wang, S.-h. Zhong, J. Peng, J. Jiang, and Y. Liu, "Data augmentation for eeg-based emotion recognition with deep convolutional neural networks," in *International Conference on Multimedia Modeling*. Springer, 2018, pp. 82–93.

[6] I. Goodfellow, J. Pouget-Abadie, M. Mirza, B. Xu, D. Warde-Farley, S. Ozair, A. Courville, and Y. Bengio, "Generative adversarial nets," in *Advances in neural information processing systems*, 2014, pp. 2672–2680.

[7] D. Li, D. Chen, B. Jin, L. Shi, J. Goh, and S.-K. Ng, "Mad-gan: Multivariate anomaly detection for time series data with generative adversarial networks," in *International Conference on Artificial Neural Networks*. Springer, 2019, pp. 703–716.

[8] Y. Luo, X. Cai, Y. Zhang, J. Xu *et al.*, "Multivariate time series imputation with generative adversarial networks," in *Advances in Neural Information Processing Systems*, 2018, pp. 1596–1607.

[9] X. Yi, E. Walia, and P. Babyn, "Generative adversarial network in medical imaging: A review," *Medical image analysis*, p. 101552, 2019.

[10] T. Mikolov, M. Karafiát, L. Burget, J. Černockỳ, and S. Khudanpur, "Recurrent neural network based language model," in *Eleventh annual conference of the international speech communication association*, 2010.

[11] T. Mikolov, A. Deoras, D. Povey, L. Burget, and J. Černockỳ, "Strategies for training large scale neural network language models," in *2011 IEEE Workshop on Automatic Speech Recognition & Understanding*. IEEE, 2011, pp. 196–201.

[12] "BCI competition 2008 - graz data set B," http://www.bbci.de/competition/iv/desc{_}2b.pdf, accessed: 2019-09-18.

[13] L. Cohen, *Time-frequency analysis*. Prentice hall, 1995, vol. 778.

[14] J. Allen, "Short term spectral analysis, synthesis, and modification by discrete fourier transform," *IEEE Transactions on Acoustics, Speech, and Signal Processing*, vol. 25, no. 3, pp. 235–238, 1977.

[15] ——, "Applications of the short time fourier transform to speech processing and spectral analysis," in *ICASSP'82. IEEE International Conference on Acoustics, Speech, and Signal Processing*, vol. 7. IEEE, 1982, pp. 1012–1015.

[16] J. B. Allen and L. R. Rabiner, "A unified approach to short-time fourier analysis and synthesis," *Proceedings of the IEEE*, vol. 65, no. 11, pp. 1558–1564, 1977.

[17] S. Roy, K. McCreadie, and G. Prasad, "Can a single model deep learning approach enhance classification accuracy of an eeg-based brain-computer interface?" in *2019 IEEE International Conference on Systems, Man and Cybernetics (SMC)*. IEEE, 2019, pp. 1317–1321.